Silicate-SiO reaction in a protoplanetary disk recorded by oxygen isotopes in chondrules

Ryoji Tanaka[1*] & Eizo Nakamura[1]

[1]The Pheasant Memorial Laboratory for Geochemistry and Cosmochemistry, Institute for Planetary Materials, Okayama University, Misasa, Tottori, 682-0193, Japan

*Corresponding author: ryoji@misasa.okayama-u.ac.jp

The formation of planetesimals and planetary embryos during the earliest stages of the solar protoplanetary disk largely determined the composition and structure of the terrestrial planets. Within a few million years (Myr) after the birth of the solar system, chondrule formation and accretion of the parent bodies of differentiated achondrites and the terrestrial planets took place in the inner protoplanetary disk[1,2]. Here we show that, for chondrules in unequilibrated enstatite chondrites, high-precision $\Delta^{17}O$ values (deviation of $\delta^{17}O$ value from a terrestrial silicate fractionation line) vary significantly (ranging from -0.49 to +0.84‰) and fall on an array with a steep slope of 1.27 on a three oxygen isotope plot. This array can be explained by reaction between an olivine-rich chondrule melt and a SiO-rich gas derived from vaporized dust and nebular gas. Our study suggests that the majority of the building blocks of planetary embryos formed by successive silicate-gas interaction processes: silicate-H_2O followed by silicate-SiO interactions under more oxidized and reduced conditions, respectively, within a few Myr after the formation of the solar system.

Major precursor components of enstatite chondrites (EC), differentiated planetesimals, Mars, and the Earth are thought to have been formed at similar heliocentric distances[3,4]. The unequilibrated EC preserve records of nebular conditions in each component (chondrules, Ca-Al-rich inclusions [CAIs], Fe-Ni-metal, and matrix), each of which has not been heavily overprinted by post-accretionary thermal processes. Thus, these components are considered reasonable analogs of the major source materials for the inner planets[5]. Oxygen isotopes of chondrules record distinct characteristics of the localized nebular environment, thus they are considered a key tracer of the nebular conditions at which planetesimal precursors formed during the earliest stages of the protoplanetary disk. Oxygen isotopic compositions for most of the bulk EC and EC chondrules resemble those of the Earth and Moon, clustered around the terrestrial fractionation line (TFL)[6-8], whereas some pyroxenes and olivines have more ^{16}O-poor and ^{16}O-rich compositions, respectively[9]. Although these data show no clear trend on the three-oxygen isotope diagram, they have been interpreted as the result of mixing processes between precursors solids including ^{16}O-rich components and nebular gas with oxygen isotopic compositions near the TFL[8,9]. However, yet uncertain are the physical and chemical parameters for the chondrule formation process, including the oxygen isotopic compositions of the nebular gas, solid/gas ratios, temperature, and the exact mixing process involved.

Oxygen isotopic compositions of individual chondrules in EC have been reported for only three EH chondrites (high-iron chemical group of EC)[6-8]. One of the reasons for the paucity of previous work is the analytical difficulty imposed by small sample sizes related to the mean diameter of chondrules in EH chondrites (0.2 mm). These chondrules are smaller than those in the other chondrite groups[10]. Recent analytical development (see detail in Methods) enables the analysis of $\Delta^{17}O$ values of silicate minerals with an order of magnitude better precision, from an order of magnitude smaller sample, than in previous studies[6-8]. Also, careful sample pretreatment eliminated analytical artifacts caused by terrestrial weathering and by isotopic fractionation during sample digestion in the presence of sulfide minerals (see detail in Methods). Here we report highly precise $^{17}O/^{16}O$ and $^{18}O/^{16}O$ of 80 fractions of chondrules and enstatite-rich fragments from 11 EC (Fig. 1; see detail in Methods and Supplementary Tables 1 and 2).

The results reveal several new observations. (1) The $\delta^{18}O$ values of chondrules and enstatites, except for silica-rich chondrule (SRC, Fig. 2), range between 5.0 and 6.0‰, a rage much narrower than that reported for bulk EC and of chondrule minerals (-5 to +6‰)[9]. (2) Chondrules in EH3 and EH4 show a wider range in $\Delta^{17}O$ (-0.489 to +0.836‰) than bulk EC (-0.41 to +0.48‰[6,11]), and their $\delta^{18}O'$ and $\delta^{17}O'$ (see definitions in Methods), except for SRC, show a linear trend with a slope of 1.27 ± 0.18 (2SE). This steep slope of >1 is distinct from that for chondrules in all chondrite groups[12], suggesting a unique formation process for the EC chondrules. (3) The chondrules in EH5 and enstatite in EH6, EL6, and EL6 show smaller variations in $\Delta^{17}O$ (-0.084 to +0.149 ‰) similar to values for bulk EC. This observation indicates that the oxygen isotope compositions of chondrules and enstatites in type 5 and 6 EC approached equilibrium values during thermal metamorphism. The chondrules in St. Mark's (EH5) show a linear slope of 0.60 ± 0.04 (2SE) slightly steeper than the mass-dependent equilibrium fractionation line (the latter with a slope of 0.5305). This implies that the diffusion of oxygen among these chondrules with initially more variable $\Delta^{17}O$ was frozen during attempts to isotopically equilibrate. (4) SRC have distinct oxygen isotopic compositions, with greater $\delta^{18}O$ (6.83‰) and relatively high $\Delta^{17}O$ (0.340‰) relative to values for the enstatite-rich chondrules and enstatites.

Petrography and the inferred crystallization path demonstrate that the SRC was a completely molten droplet (Fig. 2). The bulk composition of the SRC parental melt (Supplementary Table 3) cannot have formed, by any plausible magmatic process, from a liquid having compositions of solar or typical olivine- or pyroxene-rich chondrules. It also cannot have formed by fractional crystallization or impact melting from any known type of achondrite parent body. Silica polymorphs commonly appear in EC but are less abundant in carbonaceous and ordinary chondrites. This feature is consistent with the relative enrichment of Si/Mg ratio in bulk EC compared with bulk carbonaceous and ordinary chondrites[13]. Silica-enrichments during chondrule formation process can be explained by the addition of SiO_2 into the Mg-rich chondrule by a reaction with SiO gas, one of the dominant gas species in the hot inner solar nebula[14-16]. High partial pressures of SiO in the gas phase favor high silica activity in chondrule melts, enabling the formation of silica minerals[15]. Therefore, the SRC could have been formed via reaction of molten Mg-rich chondrules with SiO vapor under high temperature conditions, >~1960 K (Fig. 2d). The association of silica-keilite in the mantle region of the SRC also suggests a gas-melt interaction process, at high partial pressures of SiO, and formation at high temperatures[17,18]. Because of the inferred high Si activity and high temperatures, the possibility of oxygen isotopic fractionation between SiO and O_2 can be eliminated, and oxygen isotopic composition of the silica polymorph should thus reflect that of the SiO gas[14]. Thus, a mass-balance calculation demonstrates that the oxygen isotope compositions ($\delta^{18}O$, $\delta^{17}O$) of the nebular gas and precursor chondrules were greater than (21.0‰, 20.0‰) and smaller than (5.0‰, 1.5‰), respectively, based on the following plausible assumptions: (i) All MgO and SiO_2 in the SRC were derived from forsterite (Mg_2SiO_4) in the precursor chondrules and SiO and O_2 in the nebula gas. (ii) The oxygen isotopic composition of the nebular gas was on the Young and Russell (YR) line representing the mixing between ^{16}O-rich and ^{16}O-poor reservoirs in the nebula[19,20]. (iii) The oxygen isotopic composition of the precursor chondrule was that of the olivine and olivine-rich chondrules in carbonaceous chondrites. More details regarding these assumptions and the procedures for calculations are presented in Methods. This is one

solution to explain the data, but the oxygen isotopic composition determined for the gas reservoir is consistent with that estimated based on the calculated compositions of chondrules in carbonaceous chondrites for exchange with 50-70% H_2O gas[21].

The presence of relict olivine within enstatite in EH3 and EH4 chondrules, and the mechanism of formation of the SRC confirm that the enstatite-rich chondrules were formed by reaction between olivine-rich chondrule melt and SiO from the nebular gas[16]. To explain the oxygen isotope variation of EH3 and EH4 chondrules, model calculations were performed using an evaporation-driven gas–melt interaction model[20] involving reaction between SiO-rich vapor and precursor dust (see the details in Methods). In this model, the oxygen isotopic composition of enstatite-rich chondrules depends on four parameters: (i) isotopic compositions of the precursor dust, (ii) isotopic composition of initial gas, (iii) dust/gas ratio (R), and (iv) temperature (T). For the calculation, parameters (i) and (ii) which have already been determined by that of SRC are used. The results (Fig. 3 and Supplementary Table 4) show that most of the chondrules have formed with R values between 8 and 2.4 at 1000 to 1600 K when the $\delta^{18}O$ of precursor olivine is given as 5‰. Even when the $\delta^{18}O$ of the precursor olivine decreased to 3‰, the R values (6.3 – 3.5) and T (1000 – 2000K) do not change significantly. The contribution of oxygen from the gas phase to the reacting chondrule melt strongly depends on R and the duration of the reaction[16,21,22]. Relatively low R values (e.g., $\sim 12 < R < \sim 100$ at total pressures of 10^{-3} bar) are required to attain the highly reduced condition indicated by the mineralogy and the low FeO in enstatite (typically FeO < 0.8 wt.%) in the EH3 and EH4 chondrules[22]. The estimated R values are much lower than that implied by chondrule melt stability[22,23]. This may indicate that the chondrule melt was not entirely thermodynamically equilibrated with the surrounding gas because of the transient nature of the vaporization and re-condensation processes. The significantly smaller mean diameter and greater proportions of completely melted chondrules in EH chondrites, relative to other chondrite groups[10], is consistent with this melting and partial vaporization processes. We conclude, therefore, that the oxygen isotopic compositions of EC chondrules preserve a record of reaction process between partially vaporized melt and highly reduced gas including SiO at relatively low gas/dust ratios.

This study has revealed that the $\Delta^{17}O$ values of EC chondrules span not only the ranges of for Earth and the Moon but also the entire range of differentiated meteorites (Fig. 3). Because oxygen constitutes >30 wt.% of rocky planetary materials, this isotopic coincidence strongly constrains their close genetic linkage in obtaining their major components. The precursor planetesimals of rocky planetary bodies are generally thought to have accreted from various mixtures of materials broadly similar to chondrites[5]. However, accretion ages of the parental bodies of the obtainable chondrites are younger than those of differentiated meteorites[1,24]. Thus, it is unlikely that the parental bodies of chondrites themselves are identical to the source materials of the differentiated planetary bodies. Nevertheless, the chondrules and other nebular components remain the best available analogues for the source materials of the differentiated planetary bodies, in that they originated in similar or various nebular reservoirs as evidenced by oxygen isotopic compositions as well as other stable isotopic systems[2,25]. The overlap in oxygen isotopic compositions suggest that the major source materials for these differentiated planetary bodies were formed by processes similar to those responsible for the EC chondrules, namely, combinations of dust evaporation and silicate-SiO interaction processes in the early

inner disk. The lower $\delta^{18}O$ value for most of the differentiated achondrites at a given $\Delta^{17}O$, relative to values for EC chondrules, may be due to melt extraction after accretion, because the $\delta^{18}O$ values of the minerals in residues of partial melting generally show decrease[26]. $\Delta^{17}O$ values for primitive achondrites such as acapulcoites-lodranites are lower than those for the EC chondrules and show large variation (Fig. 3). Their variation in $\Delta^{17}O$ can be explained by insufficient melt-gas interaction, under the low T and/or high R conditions during the formation of their pristine components, followed by incomplete melting process in their parent bodies.

Oxygen isotopic compositions of the CAI and olivine-rich chondrules formed at the earliest stage of Solar system were primarily controlled by fractionation of ^{16}O-rich and ^{16}O-poor reservoirs in the inner and the outer regions of the solar nebula, respectively[27]. Water removal from the inner protoplanetary disk that occurred within a few Myr after the formation of Solar system led to decreased oxygen fugacity in this region[28,29]. We infer that the variation in the oxygen isotopic compositions of EC chondrules could reflect this decreased oxygen fugacity. With increase in SiO/H_2O in the innermost region of the protoplanetary disk, silicate vaporization and melt-SiO reaction proceeded, resulting in the formation of enstatite-rich and silica-oversaturated chondrules. Over the same period, accretion of achondrite precursor bodies, followed by whole body melting, could have proceeded in the same region[1]. Dust vaporization and re-condensation also elevated the volatile elements (e.g., alkaline elements and halogens) without increasing the amount of H_2O in the reactant, a characteristic of chondrules in EH relative to other chondrite groups[13].

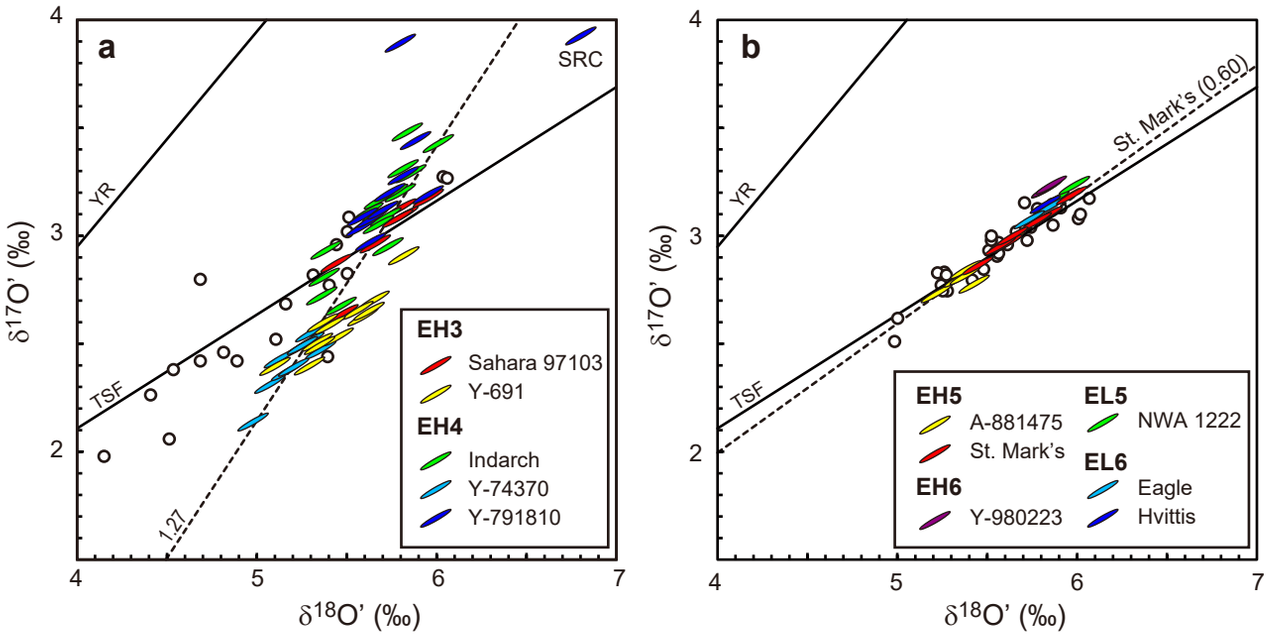

Figure 1 | Oxygen isotopic compositions of chondrule and enstatite separates from enstatite chondrites. a, chondrule(s) in EH3 and EH4. Dashed line is a regression line of EH3 and EH4 chondrules without SRC. Open circles are bulk composition of EH3 and EH4[6,11]. **b,** chondrule(s) in EH5 and enstatite separates in EH6, EL5, and EL6. Dashed line is a regression line of chondrules in St. Mark' s. Open circles are bulk composition of EH5, EH6, EL5, and EL6[6,11]. Size of symbol indicates 1σ confidence ellipse of replicated analyses of reference samples (Supplementary Table 5).

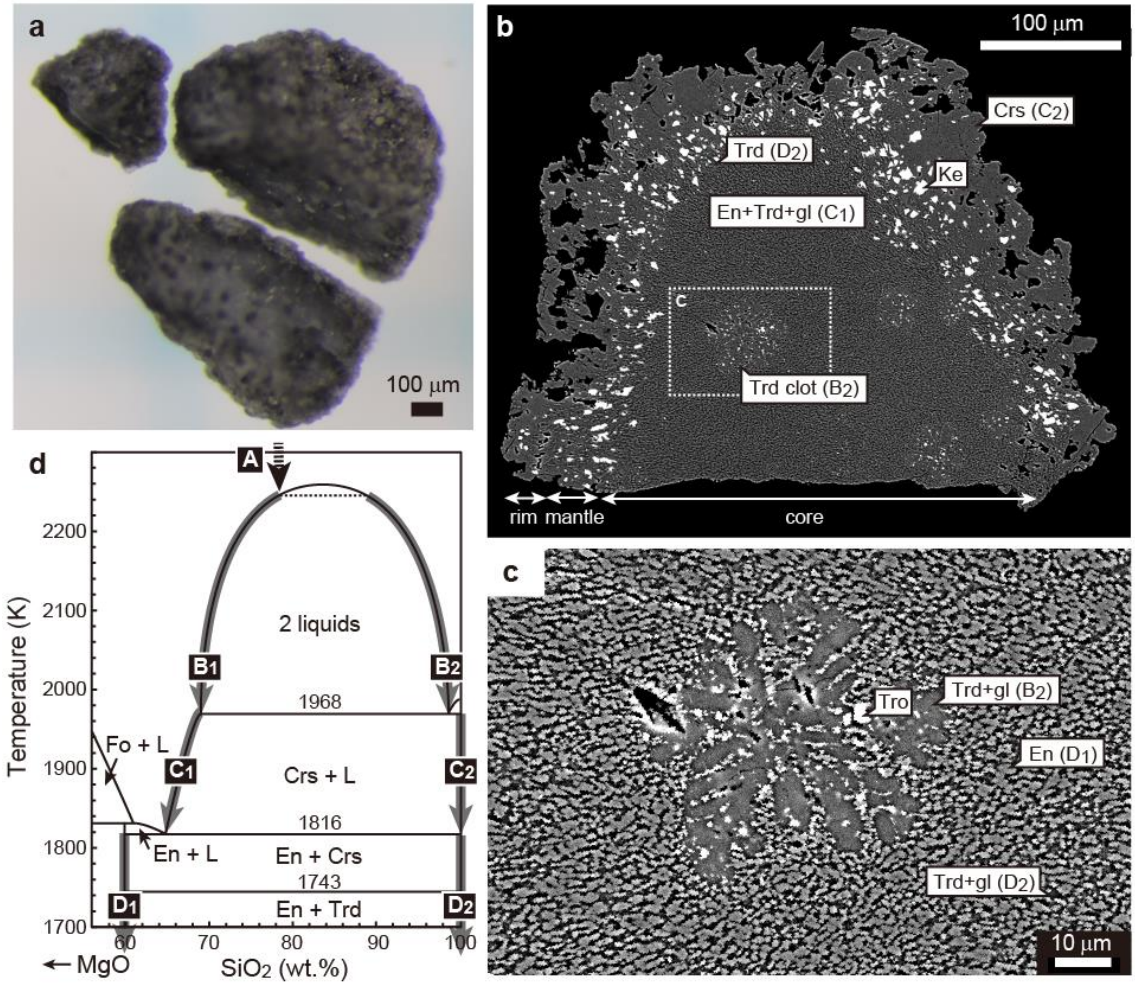

Figure 2 | Mineralogical characteristics of silica-rich chondrule (SRC). a, Photo of the SRC in Y-791810. The divided smallest fragment was used for the observation (presented in **b** and **c**) and the remaining fragments were used for O isotope analysis. **b,** Back scattered electron image of SRC. The core region is mainly composed of fine-grained (<5μm) euhedral enstatite (En) and interstitial silica-rich (SiO_2 >90wt.%) glass (gl) and tridymite (Trd) with tridymite clots. The mantle region is composed of silica-rich glass (SiO_2 > 92 wt.%), tridymite and keilite (Ke) with minor enstatite. The rim region is composed of tridymite and cristobalite (Crs) with minor amount of keilite (1.5 vol.%) and albite (<1 vol.%). **c**, Tridymite clot showing dendrite texture, which is composed of tridymite, silica-rich glass, and troilite (Tro). **d,** Crystallization process of SRC (gray thick allows) shown in binary phase diagram of MgO-SiO_2[30]. The initial composition of melt droplet (A) is determined by the bulk composition of SRC (Supplementary Table 3). The presence of two domains in the core region, MgO-rich tridymite-enstatite matrix (B_1) and SiO_2-rich tridymite clots (B_2), can be explained by solvus exsolution of the parental melt above 1968 K. After the melt cooled to 1968 K, cristobalite began crystallizing in the rim region (C_2). In the core region, SiO_2-rich immiscible melt (B_2) began crystallizing euhedral minerals in the MgO-rich melt matrix, then cristobalite began crystallizing along with keilite in the mantle region (C_2). The MgO concentration of the remaining melt (C_1) increased until the temperature cooled to the eutectic point at 1816 K. The dendritic texture of the clot (B_2) indicates its rapid crystallization. Then, the melt was exhausted leaving a mixture of enstatite (D_1) and cristobalite (D_2). Finally, cristobalite converted to tridymite, which is stable below 1743 K (D_2). Silica polymorphs were identified by micro-Raman spectra (Supplementary Fig. 2). Fo: forsterite; L: liquid.

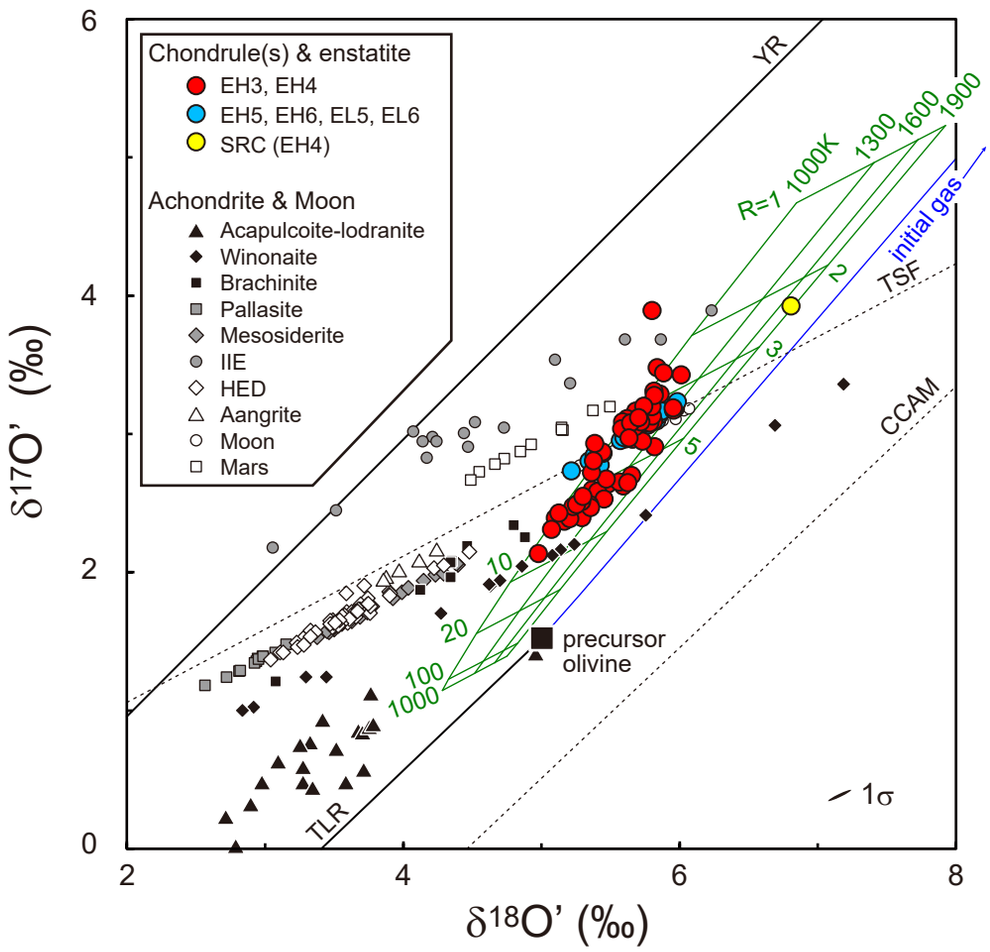

Figure 3 | Oxygen isotopic compositions of EC chondrules and enstatite. Green mesh lines show the calculated oxygen isotopic compositions of pyroxene using the model of evaporation-driven gas melt interaction[20] and the determined parameters ($\delta^{18}O$ = 5.0 ‰ and $\delta^{17}O$ = 1.5 ‰ for precursor olivine and $\delta^{18}O$ = 21.0 ‰ and $\delta^{17}O$ = 20.0 ‰ for initial solar gas) at variable temperature (in kelvin) and dust/gas ratio (R). Details regarding the methods of calculation are provided in the Methods and results are provided in Supplementary Table 4. CCAM: Carbonaceous chondrite anhydrous mineral line, TLR: Tagish Lake chondrules, isolated forsterite and isolated olivine line, YR: Young and Russel line, and TSF: Terrestrial Silicate Fractionation line. Sources of data compiled here are shown in the Methods.

Methods

Samples and Analytical procedures.

Chunk meteorite samples of Sahara 97103 (EH3), Yamato 691 (Y-691, EH3), Indarch (EH4), Yamato 74370 (Y-74370, EH4), Yamato 79810 (Y-79810, EH4), Asuka 881475 (A-881475, EH5), St. Mark's (EH5), Yamato 980223 (Y-980223, EH6), NWA 1222 (EL5), Eagle (EL6), and Hvittis (EL6) were used in this study. Indarch, NWA 1222, Eagle, and Hvittis meteorites are from the DREAM sample depository at the Institute for Planetary Materials[31], all the Antarctica meteorites were loaned from the National Institute of Polar Research in Tokyo, and the St. Mark's meteorite was loaned from Natural History Museum in Vienna. Analyzed chondrules were either porphyritic pyroxene or radial pyroxene (Supplementary Fig. 1) except for one silica-rich chondrule (SRC) (Fig. 2). The Mg# (=100×Mg/[Mg+Fe^{2+}] in mol) of enstatite in chondrules and enstatite-rich fragments, analyzed for representative samples, ranges from 98 to 100. Petrographic characteristics of enstatite-rich fragments separated from EH3, EH4, and EH5 (Supplementary Fig. 1) indicate that they are fragments of chondrules. Thus, both the chondrule and enstatite-rich fragments from these samples are referred to as "chondrule". On the other hand, chondrules underwent metamorphic recrystallization in EH6, EL5, and EL6. Thus, enstatite-rich fragments from these samples are referred to as "enstatite". Poikilitic olivine inclusions (Mg# = 99 to 100) in enstatite (< 5 % in volume) occur in porphyritic pyroxene chondrules from all EH3 and EH4, but are absent in EH5, EH6, EL5, and EH6 (Supplementary Fig. 1). These olivine inclusions have been interpreted as relics of initial condensation products that survived later reduction or melting processes that formed the surrounding enstatite[9].

The chunk samples were roughly crushed with a silicon nitride mortar and pestle. Then, chondrule and chondrule-rich fragments were hand-picked using tweezers under a binocular microscope. The chondrules and remaining fragments were then acid-leached. Newton et al.[11] leached the bulk powder of EC finds by 1M HCl, and demonstrated significant isotopic shifts between unleached and leached samples. However, those authors did not indicate whether the weathering product and sulfide minerals were completely dissolved in their acid-leached samples. In this study, sample fragments were washed using 6M HCl for a few hours until the production of reactant gas ceased, then washed more than three times with ion-exchanged water. Part of the acid-washed chondrule and pyroxene separates were observed using optical and electron microscopes. Acid-leaching does not dissolve enstatite and Na-rich plagioclase[32], which are the main constituents of the EC chondrules; however this acid-leaching completely dissolved weathered materials, Fe-Ni alloy, and troilite on the surface area of the sample fragments. Electron microprobe observations confirmed that pyroxene, plagioclase, and enclosed olivine, mesostasis, and sulfide minerals were not reacted with the HCl (Supplementary Fig. 1). Chondrules of >0.3 mg were selected for the single chondrule analysis and chondrules of <0.3 mg were combined for analyses of composite chondrules.

The fluorination and gas purification methods used for analysis are modified after Sharp[33] and details of the method have been described eleswhere[34]. The O_2 from silicate sample was extracted using a CO_2 laser with BrF_5 as an oxidation agent. The extracted O_2 was purified on the extraction line, then trapped with 13 Å molecular sieve at liquid N_2 temperature. The isotope ratios in the extracted O_2 gas were determined using a Thermo MAT253 gas source

mass spectrometer in dual inlet mode with simultaneous detection of m/z = 32, 33, and 34. The ion beams were collected in Faraday collectors attached to amplifiers with $3x10^8$, $3x10^{11}$, and $1x10^{11}$ Ω feedback resistors. For each sample, 8 blocks of 11 cycles each were measured with a total measurement time of ~ 90 min. The $^{18}O/^{16}O$ and $^{17}O/^{16}O$ of the sample is expressed as the common delta notation relative to VSMOW2 as $\delta^{17 \text{ or } 18}O = (^{17 \text{ or } 18}O/^{16}O)_{sample}/ (^{17 \text{ or } 18}O/^{16}O)_{VSMOW2} - 1$. The working reference gas was calibrated by VSMOW2 and SLAP2 just before this analytical sequence, and all data are expressed using the VSMOW2/SLAP2 scale. The results of the reference gas calibrations have been reported elsewhere[35]. The oxygen isotopic composition of the MSOL1 (in-house San Carlos olivine standard) and all data for unknowns analyzed in this study were identical between VSMOW2- and VSMOW2/SLAP2-scale within the error. The excess ^{17}O value relative to terrestrial silicate fractionation line (TSFL) is defined as $\Delta^{17}O = \delta^{17}O' - 0.527 \times \delta^{18}O'$, where $\delta^{17}O' = \ln(\delta^{17}O^* + 1)$, $\delta^{17}O^* = \delta^{17}O + 0.039 \times 10^{-3}$, and $\delta^{18}O' = \ln(\delta^{18}O + 1)$. Analytical uncertainty for the data was determined by repeat analyses of MSOL-1 analyzed every 2 to 3 analyses of unknowns (Supplementary Table 5). The intermediate precision of MSOL-1 was obtained as $\delta^{17}O = 2.754 \pm 0.035$ ‰, $\delta^{18}O = 5.288 \pm 0.072$ ‰, and $\Delta^{17}O = 0.004 \pm 0.009$ ‰ (1SD, N = 39).

Several chondrule and enstatite separates contain significant amounts of plagioclase or albitic mesostasis, up to ~10 vol. %. When the analyzed samples contain 10 wt.% of albite with 90 wt.% of enstatite, the $\delta^{18}O$ value of the mixture can be elevated by 0.11 to 0.03 ‰ when they were equilibrated between 1200 and 2000°C[36]. The deviation can exceed the 1SD external precision (0.072) if they are equilibrated at <1400 °C. However, the deviation is much smaller than the 2SD intermediate precision and also the variation in each meteorite. Thus, effects of sample impurity are regarded as being negligible in the present discussion.

Parts of the chondrule and enstatite separates were mounted in epoxy resin and polished. The major element concentrations of mineral phases were determined using a JEOL JSM-7001F SEM equipped with energy dispersive X-ray spectrometers (EDS) and Oxford INCA X-Max and X-art. The analyses were conducted at a 10 kV acceleration voltage and a 5 nA beam current, and with 100 s integration times. Silicate mineral standards were used for calibration of the quantitative analyses. The repeat analyses of San Carlos olivine mounted in the same epoxy yielded a composition of (in wt.%) $SiO_2 = 40.5 \pm 0.1$, $FeO = 9.0 \pm 0.1$, $MgO = 49.8 \pm 0.1$, $MnO = 0.11 \pm 0.07$, $NiO = 0.41 \pm 0.09$, $CaO = 0.06 \pm 0.03$, and $Mg\# = 90.8 \pm 0.1$ (N = 13, 1SD). This compositions is identical to that obtained using an electron probe micro analyzer with wavelength dispersive spectrometers[34]. The bulk composition of SRC (Supplementary Table 3) was determined by analyzing the 127 broad areas.

Identification of silica polymorphs (Supplementary Fig. 2) was accomplished by micro-Raman spectroscopy using a Thermo Scientific DXR equipped with a 532 nm Nd-YVO_4 laser and a confocal optical microscope. The laser system is equipped with grating of resolution of 3 cm^{-1} that covers the range of wavenumbers from 50 to 1800 cm^{-1}. A Raman spectrum was collected using 1 mW laser and 50 μm pinhole aperture with exposure time of 60s. The laser diameter was 0.6 μm. Spectra were processed by automatic baseline correction using the OMNIC software. Phases were identified by matching with reference Raman spectra in the RRUFF database.

Oxygen isotope fractionation of olivine during fluorination in the presence of pyrrhotite. Fluorination of sulfate minerals with BrF_5 yields low recovery of oxygen (approximately 20 – 40 %) and isotopic fractionation of the extracted oxygen from the original value because of the formation of S-O-F molecules such as SO_2F_2[37]. Enstatite chondrites contain significant amounts of sulfide minerals: the proportion of sulfur relative to oxygen expressed by f_s value (molar S/[S+O]) in EC ranges between 0.06 and 0.23 (average = 0.13 ± 0.09, 2SD)[38-40]. For the samples of enstatite chondrite, an opaque shell of troilite and Fe-Ni metal and sulfide-rich matrix, impossible to remove mechanically, often surround the separated chondrules. Thus, it is likely that sulfide contamination in EC chondrules can significantly modify the original oxygen isotopic composition during fluorination. To avoid this analytical artifact, we completely dissolved sulfide minerals on the surfaces of the separated fractions using 6M HCl. The acid-leaching treatment also effectively removed Fe-Ni metal and terrestrial weathering products. However, this method could not remove the sulfide inclusions present at up to 1.5 vol. % in the interiors of the chondrule and enstatite fractions.

In this study, we evaluated the degree of oxygen isotopic fractionation of silicate minerals in the presence of sulfide minerals. The experiment was performed using San Carlos olivine (MSOL-1, 73 - 200 μm) and pyrrhotite ($Fe_{0.92}S$, Nikolaevskiy mine, Dal'negorsk, Russia, < 100 μm) with various mixing ratios. The mixed sample was put in the Ni capsule and placed in the reaction chamber. To avoid the cross contamination and partial fluorination of pyrrhotite, only one sample was placed in each valve-closed chamber. For the same reason, no prefluorination treatment was performed. The oxygen blank in the pyrrhotite powder was negligible.

The results are shown in Supplementary Figure 3 and Supplementary Table 6. Recovery of oxygen and its isotopic composition do not change measurably when the f_s is lower than 0.1. However, when the f_s is greater than 0.12, the recovery of oxygen proportionally decreased with increasing of f_s. Oxygen recovery is ~50 % when the sample mixture has equivalent mole fraction of S and O. Oxygen isotopic compositions were also modified when f_s is greater than 0.15. The slope of $ln(\delta^{18}O + 1)$ vs. $ln(\delta^{17}O + 1)$ gave 0.519 ± 0.004 (1σ), which is near that of the kinetic mass-dependent fractionation (0.5158) rather than that of equilibrium isotope fractionation (0.5305)[41]. Thus, it appears that kinetic isotope fractionation of oxygen between O_2 and S-O-F compounds occurred during fluorination.

Our results demonstrated that the modification of oxygen isotope data by sulfide contamination is negligible for the acid-leached chondrules and enstatite fractions because of the low modal abundance of sulfide minerals (<1.5 vol. %). However, caution is necessary when bulk enstatite samples were analyzed without removing sulfide minerals. Without removal of sulfide, $\delta^{18}O$ and $\Delta^{17}O$ values of bulk samples can be modified up to ~0.7 ‰ and down to ~20 ppm, respectively.

Calculation method for open-system gas-melt interaction model.

The detailed calculation method for the determination of $\delta^i O_{pyroxene}$ values (i refers to either 17 or 18) shown in Fig. 3 is described in Marrocchi and Chaussidon[20], and will be briefly described here. This model considers the oxygen isotopic variation of the Mg-rich chondrules as resulting

from open-system gas-melt interactions between precursor silicate dust and a SiO-enriched gas in the protoplanetary disk. Enrichment of the SiO in the gas can be due to the partial melting and evaporation of silicate dust. Thus, the molar contents of Si and O and the oxygen isotopic composition of the evolved gas can be written as:

$$[Si]_{gas} = [Si]_{initial\ gas} + R \times [Si]_{dust} \quad (1)$$

$$[O]_{gas} = [O]_{initial\ gas} + R \times [O]_{dust} \quad (2)$$

$$\delta^i O_{gas} = \frac{\delta^i O_{initial\ gas} \times [O]_{initial\ gas} + R \times \delta^i O_{dust} \times [O]_{dust}}{[O]_{gas}} \quad (3)$$

where [*Si or O*]$_{gas}$, [*Si or O*]$_{initial\ gas}$, and [*Si or O*]$_{dust}$ are molar contents of Si or O in the evolved gas, initial gas, and precursor dust, respectively; R is the dust/gas ratio; and $\delta^i O_x$ is the oxygen isotopic composition in each component (gas, initial gas, and precursor dust). In a high-temperature region of the solar nebula, CO is the most dominant O-bearing molecule[42,43]. When the R value is increased, SiO becomes an important O-bearing molecule in the gas next to the CO. The fraction of O carried by SiO in the gas is defined as:

$$f_{SiO} = \frac{[SiO]}{[SiO]+[CO]} \quad (4)$$

where [*SiO*] and [*CO*] are molar contents of the gas in SiO and CO, respectively. Using the f_{SiO} value, the oxygen isotopic composition of the gas can be written as:

$$\delta^i O_{gas} = f_{SiO} \times \delta^i O_{SiO\ gas} + (1 - f_{SiO}) \times \delta^i O_{CO\ gas} \quad (5)$$

or

$$\delta^i O_{SiO\ gas} = \delta^i O_{gas} - (1 - f_{SiO}) \times \Delta^i O_{CO-SiO} \quad (6)$$

where $\Delta^i O_{CO\text{-}SiO}$ is the equilibrium isotopic fractionation of $\delta^{17\ or\ 18}O$ between CO and SiO. As SiO is the dominant Si-bearing gaseous species, the reaction of SiO into the melt and the reaction between olivine and melt can be written as[16]:

$$SiO_{(gas)} + \frac{1}{2} O_{2(gas)} = SiO_{2(melt)} \quad (7)$$

$$Mg_2SiO_{4(olivine)} + SiO_{2(melt)} = Mg_2Si_2O_{6(melt)} = Mg_2Si_2O_{6(pyroxene)} \quad (8)$$

Hence, the oxygen isotopic composition of the pyroxene is:

$$\delta^i O_{pyroxene} = \frac{2}{3}\delta^i O_{precursor\ olivine} + \frac{1}{3}\left(\Delta^i O_{pyroxene-SiO} + \delta^i O_{SiO}\right) \quad (9)$$

where

$$\delta^i O_{SiO} = \frac{\delta^i O_{initial\ gas} \times [O]_{initial\ gas} + R \times \delta^i O_{dust} \times [O]_{dust}}{[O]_{gas}} - \frac{\Delta^i O_{CO-SiO}}{1 + [SiO]/[CO]} \quad (10)$$

For the calculation, chemical compositions of CI chondrite and the Solar abundance[44] were used for the precursor dust and initial gas compositions, respectively ($[Si]_{dust} = [Si]_{initial\ gas} = 1 \times 10^6$, $[O]_{dust} = 7.55 \times 10^6$, $[O]_{initial\ gas} = 1.41 \times 10^7$, $[C]_{dust} = 7.72 \times 10^5$, and $[C]_{initial\ gas} = 7.08 \times 10^6$). The $\Delta^i O_{CO\text{-}SiO}$ and $\Delta^i O_{pyroxene\text{-}SiO}$ values were temperature-dependent fractionation factors[45].

Marrocchi and Chaussidon[20] assumed that the oxygen isotopic composition of the initial gas lies on the YR line with $\delta^{18}O = +10‰$. It is widely accepted that the oxygen isotopic composition of the nebular gas was controlled by mixing of ^{16}O-rich CO and ^{16}O-poor H_2O, which forms slope 1 line on the three oxygen isotope plot[46]. Thus, it is likely that the oxygen isotopic composition of the initial gas lies on the YR line. However, it was not clearly explained by those authors why the $\delta^{18}O$ value of the initial gas is +10‰[20]. In this study, the $\delta^i O_{initial\ gas}$ and $\delta^i O_{precursor\ olivine}$ was determined using the oxygen isotopic compositions of SRC. Proportions of SiO_2 and Mg_2SiO_4 in the SRC calculated from bulk composition (Supplementary Table 3) are 69.0 and 24.8 wt.%, respectively. Thus, contributions of oxygen in the SRC derived from the gas and chondrule melt were calculated as 76.5% and 23.5%, respectively. Thus, the $\delta^i O_{SRC}$ can be written as:

$$\delta^i O_{SRC} = 0.235 \times \delta^i O_{precursor\ olivine} + 0.765 \times \left(\Delta^i O_{SRC-SiO} + \delta^i O_{SiO}\right) \quad (11)$$

where $\delta^{18}O_{SRC} = 6.846$ and $\delta^{17}O_{SRC} = 3.943‰$ (Supplementary Table 1) and $\Delta^i O_{SRC\text{-}SiO}$ is temperature-dependent fractionation factor between SRC and SiO. Since the SRC was achieved at >~1970 K (Fig. 2), $\Delta^i O_{SRC\text{-}SiO}$ can be calculated by the $\Delta^i O_{pyroxene\text{-}SiO}$ and $\Delta^i O_{quartz\text{-}SiO}$ at 2000K[45] using the molar fractions of $MgSiO_3$ and SiO_2 in the bulk SRC.

Since $\delta^i O_{initial\ gas}$ is on the YR line:

$$\ln\left(\delta^{17}O_{initial\ gas} + 1\right) = \ln\left(\delta^{18}O_{initial\ gas} + 1\right) - 1.04 \times 10^{-3} \quad (12)$$

For the $\delta^i O_{precursor\ olivine}$, Tagish Lake chondrules, isolated forsterite and isolated olivine (TLR) line which were precisely determined by a laser fluorination method[47] was used as:

$$\ln\left(\delta^{17}O_{precursor\ olivine}+1\right)=0.953\times\ln\left(\delta^{18}O_{precursor\ olivine}+1\right)-3.24\times10^{-3}\ (13)$$

and

$$\delta^{18}O_{precursor\ olivine}\leq 5\ ‰\ (14)$$

Although the oxygen isotopic compositions of bulk Tagish Lake meteorite was modified by asteroidal aqueous alteration, the compositions of olivine and forsterite grains preserve nebular conditions[47]. These data do not differ within error from those defined for the anhydrous mineral separates from Murchison chondrite[48] and primitive chondrule minerals line determined by in-situ analyses of chondrule minerals[49]. By solving equations (11) to (14), the $\delta^{17}O_{initial\ gas}$, $\delta^{18}O_{initial\ gas}$, $\delta^{17}O_{precursor\ olivine}$ and R values were calculated for a given $\delta^{i}O_{precursor\ olivine}$ value. When the $\delta^{18}O_{precursor\ olivine}$ are 5, 4, and 3‰, the $\delta^{18}O_{initial\ gas}$ values are calculated as 21.0, 29.0, and 39.9 ‰, respectively, and the R values as 8.0, 8.3. and 9.3, respectively.

The result of $\delta^{i}O_{pyroxene}$ values (Equation 9) at $\delta^{18}O_{precursor\ olivine}$ = 5 calculated for varying dust/gas ratio (*R*) and temperature (T) ranges as shown in Supplementary Table 4 and Fig. 3.

Data compilation for O isotopic compositions of achondrites. Data sources of oxygen isotopic compositions of achondrite and Lunar samples shown in Fig. 3 are: Acaplucoite-lodranite[50], winonaite[51], brachinite[51], pallasite[52], mesosiderite[52], IIE[53], HED[50,54], angrite[50], Lunar[55,56], and Mars[57]. Because the measurements of the $\delta^{18}O$ and $\delta^{17}O$ values of San Carlos olivine, UWG-2, and NBS-28 of ref. 57 are systematically lower than those in our study, their data were recalculated by adding +0.295 ‰ and +0.184 ‰ for $\delta^{18}O$ and $\delta^{17}O$ values, respectively.

Data availability

The data that support the plots within this paper and other findings of this study are available from the corresponding author upon reasonable request.

References

1 Kleine, T. *et al.* Hf–W chronology of the accretion and early evolution of asteroids and terrestrial planets. *Geochim. Cosmochim. Acta* **73,** 5150-5188 (2009).

2 Connelly, J. N. *et al.* Absolute chronology and thermal processing of solids in the solar protoplanetary disk. *Science* **338,** 651-655 (2012).

3 Clayton, R. N., Onuma, N. & Mayeda, T. K. A classification of meteorites based on oxygen isotopes. *Earth Planet. Sci. Lett.* **30,** 10-18 (1976).

4 Warren, P. H. Stable-isotopic anomalies and the accretionary assemblage of the Earth and Mars: A subordinate role for carbonaceous chondrites. *Earth Planet. Sci. Lett.* **311,** 93-100 (2011).

5 Lodders, K. An oxygen isotope mixing model for the accretion and composition of rocky planets. *Space Sci. Rev.* **92,** 341-354 (2000).

6 Clayton, R. N., Mayeda, T. K. & Rubin, A. E. Oxygen isotopic compositions of enstatite chondrites and aubrites. *J. Geophys. Res. Solid Earth* **89,** C245-C249 (1984).

7 Clayton, R. N. & Mayeda, T. K. Oxygen isotopes in chondrules from enstatite chondrites: Possible identification of a major nebular reservoir. *Lunar and Planetary Science XVI.* 142-143 (1985).

8 Clayton, R. N., Mayeda, T. K., Goswami, J. N. & Olsen, E. J. Oxygen isotope studies of ordinary chondrites. *Geochim. Cosmochim. Acta* **55,** 2317-2337 (1991).

9 Weisberg, M. K. *et al.* Petrology and oxygen isotope compositions of chondrules in E3 chondrites. *Geochim. Cosmochim. Acta* **75,** 6556-6569 (2011).

10 Rubin, A. E. Petrologic, geochemical and experimental constraints on models of chondrule formation. *Earth-Sci. Rev.* **50,** 3-27 (2000).

11 Newton, J., Franchi, I. A. & Pillinger, C. T. The oxygen-isotopic record in enstatite meteorites. *Meteorit. Planet. Sci.* **35,** 689-698 (2000).

12 Franchi, I. A. Oxygen isotopes in asteroidal materials. *Rev. Mineral. Geochem.* **68,** 345-397 (2008).

13 Davis, A. M. Volatile evolution and loss. in *Meteorites and the Early Solar System II* (eds D. S. Lauretta & H. Y. McSween Jr.) 295-307 (University of Arizona Press, 2006).

14 Chaussidon, M., Libourel, G. & Krot, A. N. Oxygen isotopic constraints on the origin of magnesian chondrules and on the gaseous reservoirs in the early Solar System. *Geochim. Cosmochim. Acta* **72,** 1924-1938 (2008).

15 Libourel, G., Krot, A. N. & Tissandier, L. Role of gas-melt interaction during chondrule formation. *Earth Planet. Sci. Lett.* **251,** 232-240 (2006).

16 Tissandier, L., Libourel, G. & Robert, F. Gas-melt interactions and their bearing on chondrule formation. *Meteorit. Planet. Sci.* **37,** 1377-1389 (2002).

17 Marrocchi, Y. & Libourel, G. Sulfur and sulfides in chondrules. *Geochim. Cosmochim. Acta* **119,** 117-136 (2013).

18 Piani, L., Marrocchi, Y., Libourel, G. & Tissandier, L. Magmatic sulfides in the porphyritic chondrules of EH enstatite chondrites. *Geochim. Cosmochim. Acta* **195,** 84-

99 (2016).

19 Young, E. D. & Russell, S. S. Oxygen reservoirs in the early solar nebula inferred from an Allende CAI. *Science* **282,** 452-455 (1998).

20 Marrocchi, Y. & Chaussidon, M. A systematic for oxygen isotopic variation in meteoritic chondrules. *Earth Planet. Sci. Lett.* **430,** 308-315 (2015).

21 Di Rocco, T. & Pack, A. Triple oxygen isotope exchange between chondrule melt and water vapor: an experimental study. *Geochim. Cosmochim. Acta* (2015).

22 Ebel, D. S. & Grossman, L. Condensation in dust-enriched systems. *Geochim. Cosmochim. Acta* **64,** 339-366 (2000).

23 Alexander, C. M. O. D., Grossman, J. N., Ebel, D. S. & Ciesla, F. J. The formation conditions of chondrules and chondrites. *Science* **320,** 1617-1619 (2008).

24 Sugiura, N. & Fujiya, W. Correlated accretion ages and ε^{54}Cr of meteorite parent bodies and the evolution of the solar nebula. *Meteorit. Planet. Sci.***49,** 772-787 (2014).

25 Olsen, M. B. *et al.* Magnesium and ^{54}Cr isotope compositions of carbonaceous chondrite chondrules – Insights into early disk processes. *Geochim. Cosmochim. Acta* **191,** 118-138 (2016).

26 Eiler, J. M. Oxygen isotope variations of basaltic lavas and upper mantle rocks. *Rev. Mineral. Geochem.* **43,** 319-364 (2001).

27 Clayton, R. N. Oxygen isotopes in meteorites. *Annu. Rev. Earth Planet. Sci.* **21,** 115-149 (1993).

28 Krot, A. N., Fegley, B. J., Lodders, K. & Palme, H. in *Protostars and Planets IV* (eds V. Mannings, A. P. Boss, & S. S. Russell) 1019-1054 (University of Arizona Press, 2000).

29 Ciesla, F. J. & Cuzzi, J. N. The evolution of the water distribution in a viscous protoplanetary disk. *Icarus* **181,** 178-204 (2006).

30 Greig, J. W. Immiscibility in silicate melts; Part I. *Am J Sci* Series 5 **Vol. 13,** 1-44 (1927).

31 Yachi, Y., Kitagawa, H., Kunihiro, T. & Nakamura, E. Software dedicated for the curation of geochemical data sets in analytical laboratories. *Geostand. Geoanal. Res.* **38,** 95-102 (2014).

32 Tanaka, R. *et al.* Evaluation of the applicability of acid leaching for the ^{238}U–^{230}Th internal isochron method. *Chem. Geol.* **396,** 255-264 (2015).

33 Sharp, Z. D. A laser-based microanalytical method for the in site determination of oxygen isotope ratios of silicates and oxides. *Geochim. Cosmochim. Acta* **54,** 1353-1357 (1990).

34 Tanaka, R. & Nakamura, E. Determination of ^{17}O-excess of terrestrial silicate/oxide minerals with respect to Vienna Standard Mean Ocean Water (VSMOW). *Rapid Commun. Mass Spectrom.* **27,** 285-297 (2013).

35 Pack, A. *et al.* The oxygen isotope composition of San Carlos olivine on the VSMOW2-SLAP2 scale. *Rapid Commun. Mass Spectrom.* **30,** 1495-1504 (2016).

36 Zheng, Y.-F. Calculation of oxygen isotope fractionation in anhydrous silicate minerals.

Geochim. Cosmochim. Acta **57,** 1079-1091 (1993).

37 Bao, H. & Thiemens, M. H. Generation of O_2 from $BaSO_4$ using a CO_2–laser fluorination system for simultaneous analysis of $\delta^{18}O$ and $\delta^{17}O$. *Anal. Chem.* **72,** 4029-4032 (2000).

38 Keil, K. Mineralogical and chemical relationships among enstatite chondrites. *J. Geophys. Res.* **73,** 6945-6976 (1968).

39 Zhang, Y., Benoit, P. H. & Sears, D. W. G. The classification and complex thermal history of the enstatite chondrites. *J. Geophys. Res.: Planets* **100,** 9417-9438 (1995).

40 Weisberg, M. K. et al. EH3 and EL3 chondrites: A petrologic-oxygen isotopic study. in *Lunar and Planetary Science Conference XXVI.* 1481-1482 (1995).

41 Young, E. D., Galy, A. & Nagahara, H. Kinetic and equilibrium mass-dependent isotope fractionation laws in nature and their geochemical and cosmochemical significance. *Geochim. Cosmochim. Acta* **66,** 1095-1104 (2002).

42 Bergin, E. A. *et al.* Implications of submillimeter wave astronomy satellite observations for interstellar chemistry and star formation. *Astrophys. J. Lett.* **539,** L129-L132 (2000).

43 Marechal, P., Viala, Y. P. & Benayoun, J. J. Chemistry and rotational excitation of O-2 in interstellar clouds .1. Predicted emissivities of lines for the ODIN, SWAS, PRONAOS-SMH and PIROG 8 submillimeter receivers. *Astron. Astrophys.* **324,** 221-236 (1997).

44 Lodders, K. Solar System Abundances and Condensation Temperatures of the Elements. *Astrophys. J.* **591,** 1220 (2003).

45 Javoy, M. *et al.* First-principles investigation of equilibrium isotopic fractionation of O- and Si-isotopes between refractory solids and gases in the solar nebula. *Earth Planet. Sci. Lett.* **319–320,** 118-127 (2012).

46 Young, E. D. *et al.* Mass-independent oxygen isotope variation in the solar nebula. *Rev. Mineral. Geochem.* **68,** 187-218 (2008).

47 Russell, S. D. J., Longstaffe, F. J., King, P. L. & Larson, T. E. The oxygen-isotope composition of chondrules and isolated forsterite and olivine grains from the Tagish Lake carbonaceous chondrite. *Geochim. Cosmochim. Acta* **74,** 2484-2499 (2010).

48 Clayton, R. N. & Mayeda, T. K. The oxygen isotope record in Murchison and other carbonaceous chondrites. *Earth Planet. Sci. Lett.* **67,** 151-161 (1984).

49 Ushikubo, T., Kimura, M., Kita, N. T. & Valley, J. W. Primordial oxygen isotope reservoirs of the solar nebula recorded in chondrules in Acfer 094 carbonaceous chondrite. *Geochim. Cosmochim. Acta* **90,** 242-264 (2012).

50 Greenwood, R. C., Franchi, I. A., Jambon, A. & Buchanan, P. C. Widespread magma oceans on asteroidal bodies in the early Solar System. *Nature* **435,** 916-918 (2005).

51 Greenwood, R. C., Franchi, I. A., Gibson, J. M. & Benedix, G. K. Oxygen isotope variation in primitive achondrites: The influence of primordial, asteroidal and terrestrial processes. *Geochim. Cosmochim. Acta* **94,** 146-163 (2012).

52 Greenwood, R. C. *et al.* Oxygen isotope variation in stony-iron meteorites. *Science* **313,** 1763-1765 (2006).

53 McDermott, K. H. *et al.* Oxygen isotope and petrological study of silicate inclusions in IIE iron meteorites and their relationship with H chondrites. *Geochim. Cosmochim. Acta* **173,** 97-113 (2016).

54 Wiechert, U. H., Halliday, A. N., Palme, H. & Rumble, D. Oxygen isotope evidence for rapid mixing of the HED meteorite parent body. *Earth Planet. Sci. Lett.* **221,** 373-382 (2004).

55 Herwartz, D., Pack, A., Friedrichs, B. & Bischoff, A. Identification of the giant impactor Theia in lunar rocks. *Science* **344,** 1146-1150 (2014).

56 Young, E. D. *et al.* Oxygen isotopic evidence for vigorous mixing during the Moon-forming giant impact. *Science* **351,** 493-496 (2016).

57 Franchi, I. A., Wright, I. P., Sexton, A. S. & Pillinger, C. T. The oxygen-isotopic composition of Earth and Mars. *Meteorit. Planet. Sci.* **34,** 657-661 (1999).

Reference

58 Kihara, K., Hirose, T. & Shinoda, K. Raman spectra, normal modes and disorder in monoclinic tridymite and its higher temperature orthorhombic modification. *J. Miner. Petrol. Sci.* **100,** 91-103 (2005).

Acknowledgements

We thank Matthew R. M. Izawa, Yuri Shimaki, Tak Kunihiro, and Gray E. Bebout for their constructive suggestions that improved this paper. We also thank Yuri Shimaki and Kayo Tanaka for assistance in the laboratory. We are grateful for the loan of the meteorites from the National Institute of Polar Research and Natural History Museum in Vienna. This study was partly supported by JSPS KAKENHI Grant Number 16K05578.

Author Contributions

R.T. designed the study, analyzed data and wrote the paper. E.N. was involved in study design. All authors discussed the result and commented on the manuscript.

Competing financial interests

The authors declare no competing financial interests.

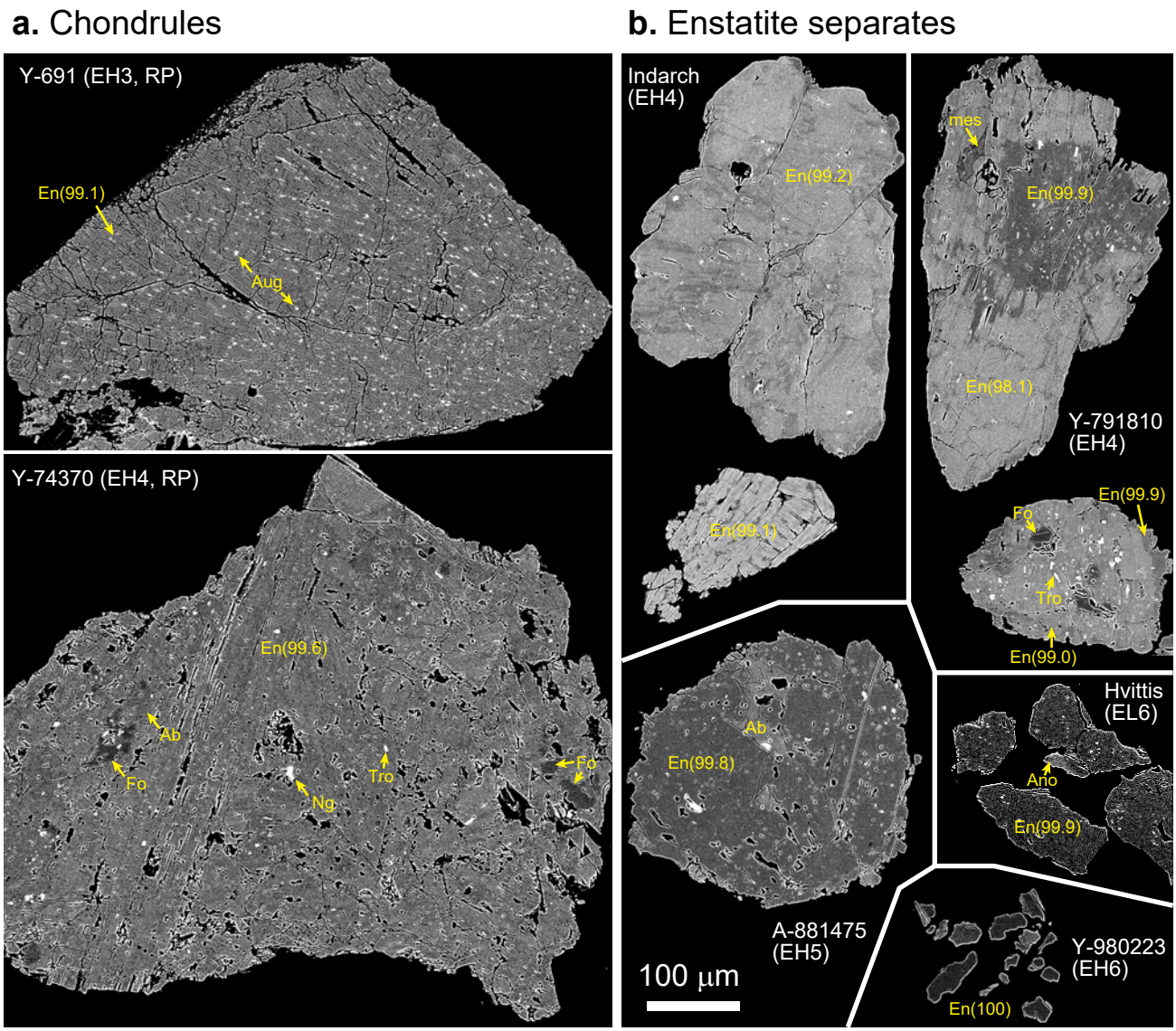

Supplementary Figure 1 | Back scattered electron images of separated and acid-leached chondrule fragment (a) and enstatite-rich fraction (b). En: enstatite, Aug: augite; Ab: albite, Ng: niningerite, Tro: troilite, Fo: forsterite, mes: mesostasis, Ano: anorthoclase. Number indicates Mg# of enstatite.

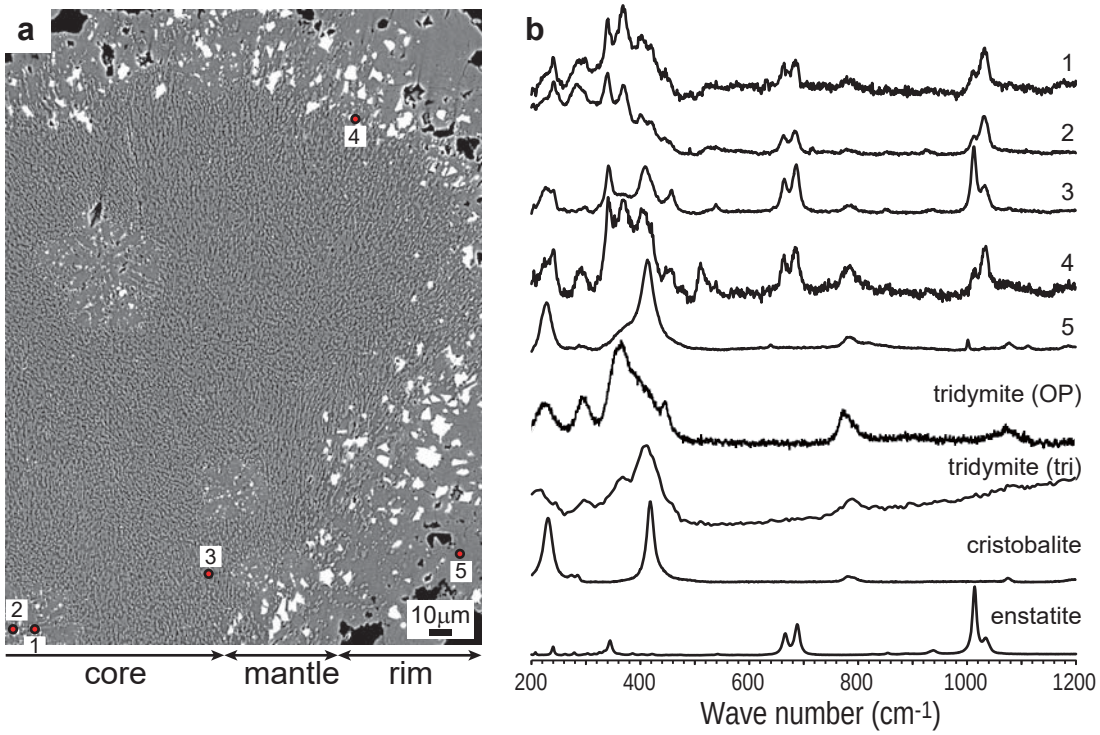

Supplementary Figure 2 | Raman spectra of silica-rich chondrule (SRC). a, Back scattered electron (BSE) image of SRC (Y791810-Ch6). Red circles with number indicates the analyzed point for Raman spectra. **b,** Raman spectra of SiO_2 phases in SRC. [1] and [2] orthorhombic tridymite, enstatite, and amorphous phase in the tridymite clot, [3] triclinic tridymite and enstatite peaks in the matrix of core region, [4] orthorhombic tridymite, amorphous phase, and enstatite peaks in the mantle region, and [5] cristobalite peaks in the rim region. Reference Raman spectra of orthorhombic tridymite (OP)[58], triclinic tridymite (RRUFFID = R040143), cristobalite (RRUFFID = X050046), and orthoenstatite are also shown.

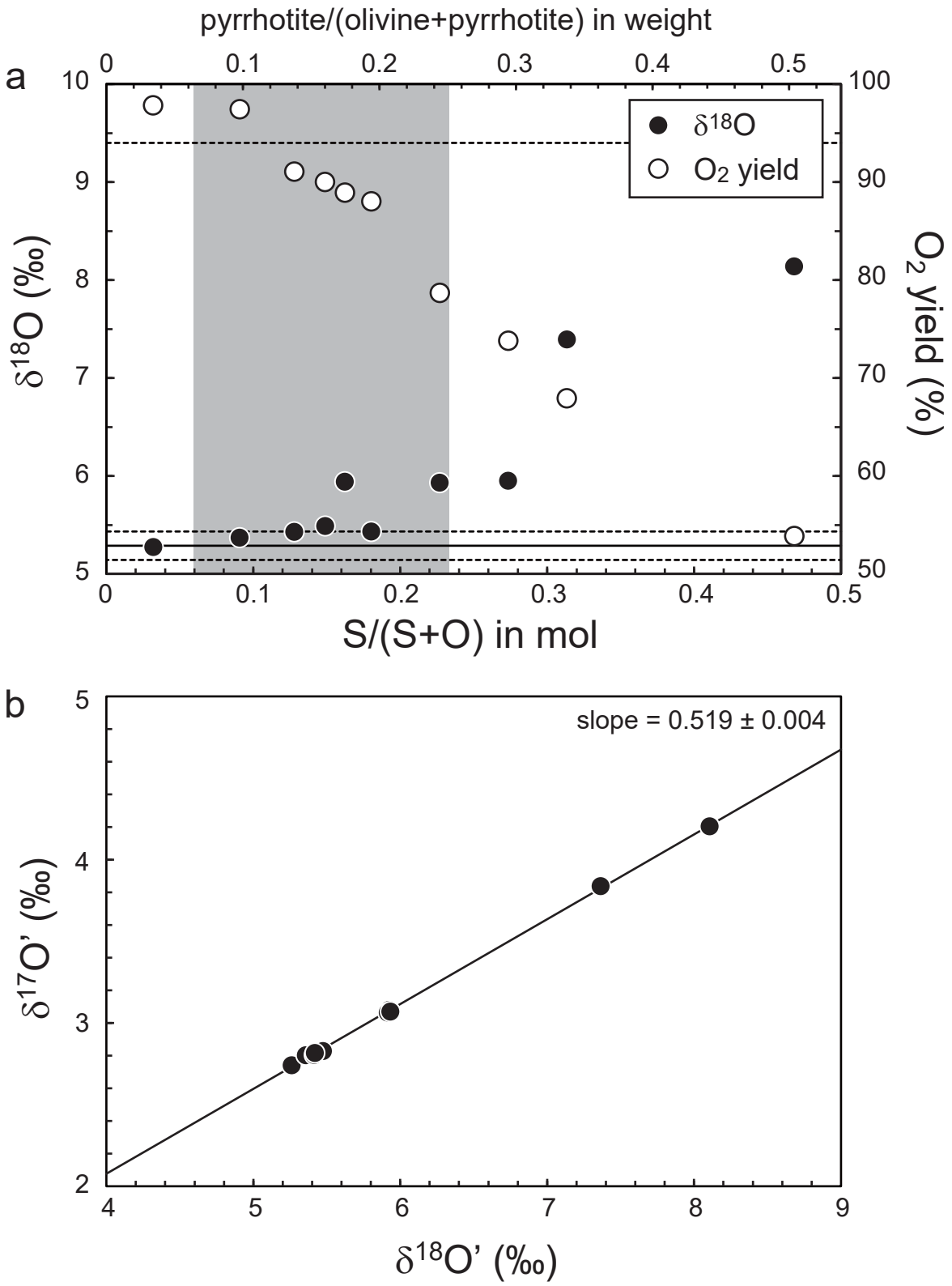

Supplementary Figure 3 | Oxygen isotopic data of San Carlos olivine (MSOL-1) – pyrrhotite mixture. a, The $\delta^{18}O$ value and recovery of oxygen from MSOL-1 and pyrrhotite mixture with various mixing ratios. The solid and broken lines are average values and 2SD analytical uncertainties, respectively, for $\delta^{18}O$ value and recovery yield determined by repeated analyses of MSOL-1. The shaded area indicates the range of S/(S+O) for bulk enstatite chondrites calculated from the modal abundance data[38-40]. **b,** The slope of $\delta^{18}O'$ vs. $\delta^{17}O'$ for the MSOL-1 and pyrrhotite mixtures

Supplementary Table 1 | Oxygen isotopic composition of chondrules and enstatite separates in EH3 and EH4 chondrites.

sample†	number of grain	type‡	diameter (mm)	weight for analysis (mg)	$\delta^{18}O$ (‰)		$\delta^{17}O$ (‰)		$\delta^{17}O^*$ (‰)	$\Delta^{17}O_{TSFL}$ (‰)	
Sahara 97103 (EH3)											
WR				1.87	6.245	(4)	3.265	(10)	3.298	0.011	(9)
Ch1	1	PP	1.22	0.65	5.845	(6)	3.072	(13)	3.105	0.029	(13)
Ch comp1	5	PP	0.54-0.68	0.63	5.509	(7)	2.615	(12)	2.648	-0.251	(12)
Ch comp2	12	PP	0.26-0.72	0.62	5.690	(6)	2.940	(5)	2.973	-0.022	(5)
En1	nc	-	0.16-0.66	0.57	5.989	(4)	3.152	(9)	3.185	0.034	(9)
En2	nc	-	0.14-0.56	0.69	5.817	(4)	3.059	(5)	3.092	0.030	(5)
En3	nc	-	0.18-0.52	0.47	5.834	(4)	3.108	(9)	3.141	0.070	(9)
En4	nc	-	0.07-0.25	1.07	5.470	(5)	2.849	(10)	2.882	0.003	(8)
Y-691 (EH3)											
Ch1	1	PP	0.92	0.47	5.366	(5)	2.482	(8)	2.514	-0.309	(9)
Ch2	1	RP	1.5	0.42	5.322	(4)	2.371	(13)	2.403	-0.396	(12)
Ch3	1	RP	0.79	0.45	5.621	(4)	2.600	(6)	2.633	-0.325	(6)
Ch4	1	PP	1.08	0.34	5.395	(9)	2.572	(6)	2.604	-0.235	(10)
Ch5	1	PP	1.1	0.36	5.436	(7)	2.561	(13)	2.594	-0.267	(9)
Ch comp1	2	PP	0.83-1.10	0.30	5.127	(19)	2.368	(42)	2.401	-0.297	(17)
Ch comp2	21	-	0.40-0.57	0.50	5.683	(4)	2.678	(9)	2.711	-0.279	(9)
Ch comp3	9	-	0.30-1.0	0.54	5.482	(7)	2.506	(6)	2.538	-0.346	(5)
Ch comp4	7	-	0.43-0.60	0.40	5.378	(7)	2.466	(8)	2.499	-0.331	(8)
Ch comp5	24	-	0.18-0.54	0.42	5.594	(6)	2.630	(11)	2.663	-0.280	(13)
En1	nc	-	0.07-0.2	0.52	5.655	(2)	2.626	(8)	2.659	-0.317	(9)
En2	nc	-	0.07-0.2	0.45	5.850	(4)	2.885	(9)	2.917	-0.161	(9)
Indarch (EH4)											
WR				1.44	5.490	(3)	2.945	(12)	2.978	0.089	(11)
WR (EATG)		-	-	1.44	5.443	(3)	2.861	(6)	2.894	0.029	(12)
Ch1	1	PP	1.9	0.70	5.637	(5)	3.035	(6)	3.068	0.101	(6)
Ch2	1	PP	1.04	0.47	5.787	(4)	3.176	(9)	3.209	0.162	(10)
Ch3	1	RP	1.1	0.46	5.498	(4)	2.650	(6)	2.682	-0.211	(5)
Ch4	1	PP	0.72	0.41	6.045	(11)	3.408	(19)	3.441	0.259	(18)
Ch5	1	PP	0.64	0.37	5.390	(11)	2.698	(7)	2.730	-0.106	(7)
Ch6	1	PP	0.64	0.37	5.404	(12)	2.784	(12)	2.817	-0.027	(11)
Ch comp1	2	PP	0.64-0.70	0.45	5.762	(4)	2.927	(10)	2.960	-0.073	(10)
Ch comp2	25	-	0.18-0.36	0.50	5.890	(12)	3.267	(16)	3.300	0.200	(10)
Ch comp3	2	PP	0.53-0.57	0.37	5.831	(7)	3.178	(5)	3.211	0.142	(4)
Ch comp4	3	PP	0.60-0.74	0.54	5.847	(5)	3.290	(9)	3.323	0.245	(11)
Ch comp5	3	RP	0.63-0.70	0.37	5.705	(4)	3.086	(13)	3.119	0.116	(13)
Ch comp6	3	PP	0.54-0.74	0.43	5.870	(6)	3.461	(7)	3.494	0.403	(8)
Ch comp7	74	-	0.07-0.31	0.40	5.414	(8)	2.910	(15)	2.943	0.093	(14)
En1	7	-	0.38-0.66	0.53	5.708	(4)	3.030	(14)	3.062	0.058	(12)
En2	17	-	0.24-0.54	0.52	5.750	(4)	3.066	(6)	3.099	0.072	(7)
En3	nc	-	0.18-0.48	1.12	5.714	(4)	3.144	(12)	3.177	0.169	(13)
En4	nc	-	0.30-0.34	1.02	5.649	(4)	3.089	(5)	3.122	0.149	(7)
Y-74370 (EH4)											
Ch1	1	PP	0.87	0.57	5.384	(4)	2.445	(10)	2.478	-0.355	(9)
Ch2	1	PP	0.97	0.52	5.193	(6)	2.344	(5)	2.377	-0.355	(5)
Ch3	1	RP	1.5	0.57	5.004	(8)	2.110	(7)	2.142	-0.491	(7)
Ch4	1	RP	1.22	0.42	5.317	(10)	2.486	(10)	2.519	-0.279	(10)
Ch5	1	PP	0.9	0.42	5.232	(5)	2.365	(10)	2.398	-0.355	(10)
Ch comp1	21	-	0.20-0.36	0.63	5.255	(5)	2.452	(3)	2.485	-0.280	(4)
Ch comp2	4	PP	0.60-0.62	0.53	5.281	(7)	2.466	(8)	2.499	-0.280	(8)
Ch comp3	3	RP	0.66-0.76	0.44	5.099	(8)	2.285	(4)	2.317	-0.366	(4)
En1	10	-	0.26-0.60	0.64	5.328	(6)	2.525	(8)	2.558	-0.246	(10)
En2	20	-	0.32-0.64	0.55	5.152	(5)	2.403	(6)	2.436	-0.275	(5)
Y-791810 (EH4)											
Ch1	1	PP	0.88	0.51	5.831	(4)	3.876	(8)	3.909	0.837	(8)
Ch2	1	PP	0.86	0.43	5.917	(5)	3.421	(8)	3.454	0.339	(7)
Ch3	1	PP	0.7	0.51	5.987	(5)	3.169	(10)	3.202	0.051	(8)
Ch4	1	PP	0.82	0.44	5.848	(5)	3.258	(8)	3.291	0.212	(8)
SRC	1	CC	0.84	0.42	6.846	(6)	3.910	(9)	3.943	0.339	(9)
Ch comp1	3	PP	0.64-0.74	0.50	5.772	(3)	3.179	(8)	3.212	0.174	(8)
Ch comp2	9	-	0.24-0.52	0.40	5.618	(4)	3.066	(10)	3.099	0.142	(10)
En1	nc	-	0.10-0.42	0.58	5.611	(4)	3.017	(8)	3.050	0.096	(9)
En2	nc	-	0.14-0.48	0.46	5.675	(5)	3.059	(8)	3.092	0.105	(7)
En3	nc	-	0.10-0.48	0.49	5.733	(5)	3.097	(9)	3.130	0.112	(8)
En4	11	-	0.26-0.60	0.52	5.665	(4)	2.949	(9)	2.982	0.001	(9)

† WR = whole rock without leaching, WR (EATG) = whole rock washed by EATG, Ch = single chondrule, Ch comp = chondrule composite, En = enstatite separates

‡ PP = porphyritic pyroxene, RP = radial pyroxene, SRC = silica-rich chondrule,

nc = not counted, - = not analyzed

The number inside the parenthesis is a last digit of standard error (1SE).

Supplementary Table 2 | Oxygen isotopic composition of chondrules and enstatite separates in EH5, EH6, EL5, and EL6 chondrites.

sample†	number of grain	type‡	diameter (mm)	weight for analysis (mg)	$\delta^{18}O$ (‰)		$\delta^{17}O$ (‰)		$\delta^{17}O^*$ (‰)	$\Delta^{17}O_{TSFL}$ (‰)	
A-881475 (EH5)											
Ch1	1	PP	0.94	0.49	5.656	(4)	2.960	(8)	2.993	0.016	(9)
Ch comp1	2	PP	0.60-0.64	0.42	5.455	(7)	2.753	(9)	2.786	-0.084	(9)
Ch comp2	6	PP	0.36-0.48	0.41	5.405	(4)	2.794	(8)	2.826	-0.018	(9)
En1	nc	-	0.14-0.46	0.67	5.243	(3)	2.709	(13)	2.742	-0.018	(13)
En2	nc	-	0.08-0.14	0.63	5.372	(6)	2.782	(8)	2.814	-0.013	(7)
En3	nc	-	0.08-0.14	0.70	5.408	(3)	2.821	(6)	2.854	0.007	(7)
St. Mark's (EH5)											
Ch1	1	PP	0.8	0.40	5.639	(7)	2.942	(13)	2.975	0.007	(15)
Ch2	1	RP	>1.76	0.50	5.803	(5)	3.045	(6)	3.078	0.024	(5)
Ch comp1	2	PP	0.62-0.64	0.51	5.476	(6)	2.839	(7)	2.872	-0.010	(8)
Ch comp2	7	PP	0.28-0.66	0.46	5.601	(5)	2.931	(11)	2.963	0.015	(11)
Ch comp3	2	RP	>1.40	0.37	6.002	(3)	3.167	(9)	3.200	0.041	(9)
En1	5	-	0.56-0.64	0.48	5.672	(5)	2.978	(7)	3.011	0.026	(6)
En2	42	-	0.40-0.52	0.47	5.864	(4)	3.073	(11)	3.106	0.020	(11)
En3	18	-	0.20-0.60	0.43	5.626	(4)	2.951	(8)	2.984	0.023	(8)
Y-980223 (EH6)											
En1	nc	-	<0.1	0.66	5.866	(4)	3.201	(11)	3.233	0.146	(11)
En2	nc	-	<0.1	0.85	5.888	(4)	3.215	(7)	3.248	0.149	(7)
En3	nc	-	<0.1	0.83	5.862	(5)	3.196	(10)	3.229	0.144	(9)
NWA 1222 (EL5)											
WR				1.49	5.975	(4)	3.160	(6)	3.193	0.048	(7)
En1	nc	-	0.07-0.2	0.92	5.902	(6)	3.145	(12)	3.178	0.072	(12)
En2	nc	-	0.07-0.2	0.80	6.017	(4)	3.213	(5)	3.246	0.080	(7)
Eagle (EL6)											
WR				1.57	5.849	(2)	3.073	(2)	3.106	0.028	(3)
En1	nc	-	0.07-0.2	1.05	5.887	(7)	3.117	(8)	3.150	0.052	(9)
En2	nc	-	0.07-0.2	0.98	5.764	(2)	3.053	(10)	3.086	0.053	(11)
Hvittis (EL6)											
WR				1.34	5.836	(5)	3.091	(9)	3.124	0.052	(7)
En1	nc	-	0.07-0.2	1.00	5.855	(1)	3.124	(7)	3.157	0.076	(7)
En2	nc	-	0.07-0.2	1.22	5.848	(3)	3.095	(10)	3.128	0.050	(10)

† WR = whole rock without leaching, WR (EATG) = whole rock washed by EATG, Ch = single chondrule, Ch comp = chondrule composite, En = enstatite separates

‡ PP = porphyritic pyroxene, RP = radial pyroxene, SRC = silica-rich chondrule,

nc = not counted, - = not analyzed

The number inside the parenthesis is a last digit of standard error (1SE)

Supplementary Table 3 | Major element composition in core, mantle, and rim regions of SRC.

region	core*	clot	mantle	rim	bulk
vol.%†	47.6	-	19.1	33.3	
SiO_2	72.8	88.0	76.2	91.4	79.6
TiO_2	0.02	0.07	0.01	0.01	0.02
Cr_2O_3	0.04	0.13	0.25	0.14	0.12
Al_2O_3	2.50	1.29	2.18	1.39	2.07
FeO	0.18	1.09	2.63	1.33	1.03
MnO	0.06	0.21	0.61	0.28	0.24
MgO	22.1	7.2	13.7	3.2	14.2
NiO	0.03	0.04	0.01	0.03	0.03
CaO	0.42	0.14	0.38	0.11	0.31
Na_2O	1.66	1.09	1.66	0.93	1.42
K_2O	0.03	0.00	0.01	0.00	0.02
P_2O_5	0.04	0.01	0.03	0.06	0.05
S	0.13	0.79	2.32	1.14	0.88
Mg#	99.6	92.1	90.3	81.0	96.1

*Tridymite clot. The modal abundance of core region includes the tridymite clot.
†The radius of the core region is estimated as 0.33 mm, assuming that the chondrule is sphere in shape.

Supplementary Table 4 | Result of model calculations for gas-melt interactions between olivine and gas.

R	SiO/CO	f_{SiO}	$\delta^{18}O_{neb}$	$\delta^{18}O_{SiO}$	$\delta^{18}O_{pyroxene}$	$\Delta^{18}O_{px\text{-}ol}$	$\delta^{17}O_{neb}$	$\delta^{17}O_{SiO}$	$\delta^{17}O_{pyroxene}$
T=1000K									
1	0.25	0.20	15.43	9.52	6.87	1.87	13.53	10.46	4.68
2	0.35	0.26	12.73	7.23	6.11	1.11	10.43	7.57	3.72
3	0.43	0.30	11.15	5.95	5.68	0.68	8.60	5.89	3.16
5	0.55	0.35	9.36	4.57	5.22	0.22	6.53	4.04	2.54
10	0.74	0.43	7.52	3.27	4.79	-0.21	4.42	2.21	1.93
20	0.93	0.48	6.37	2.53	4.54	-0.46	3.09	1.09	1.56
100	1.20	0.55	5.29	1.92	4.34	-0.66	1.85	0.10	1.23
1000	1.28	0.56	5.03	1.78	4.29	-0.71	1.54	-0.14	1.15
T=1300K									
1	0.25	0.20	15.43	11.70	7.43	2.43	13.53	11.59	4.98
2	0.35	0.26	12.73	9.26	6.62	1.62	10.43	8.62	3.99
3	0.43	0.30	11.15	7.86	6.16	1.16	8.60	6.89	3.41
5	0.55	0.35	9.36	6.33	5.65	0.65	6.53	4.96	2.77
10	0.74	0.43	7.52	4.84	5.15	0.15	4.42	3.02	2.12
20	0.93	0.48	6.37	3.95	4.85	-0.15	3.09	1.83	1.72
100	1.20	0.55	5.29	3.16	4.59	-0.41	1.85	0.74	1.36
1000	1.28	0.56	5.03	2.98	4.53	-0.47	1.54	0.48	1.27
T=1600K									
1	0.25	0.20	15.43	12.88	7.76	2.76	13.53	12.21	5.14
2	0.35	0.26	12.73	10.37	6.92	1.92	10.43	9.20	4.14
3	0.43	0.30	11.15	8.91	6.43	1.43	8.60	7.43	3.55
5	0.55	0.35	9.36	7.30	5.89	0.89	6.53	5.46	2.89
10	0.74	0.43	7.52	5.69	5.36	0.36	4.42	3.47	2.23
20	0.93	0.48	6.37	4.72	5.04	0.04	3.09	2.23	1.82
100	1.20	0.55	5.29	3.84	4.74	-0.26	1.85	1.09	1.44
1000	1.28	0.56	5.03	3.63	4.67	-0.33	1.54	0.82	1.35
T=1900K									
1	0.25	0.20	15.43	13.59	7.95	2.95	13.53	12.58	5.25
2	0.35	0.26	12.73	11.02	7.10	2.10	10.43	9.54	4.23
3	0.43	0.30	11.15	9.53	6.60	1.60	8.60	7.76	3.64
5	0.55	0.35	9.36	7.87	6.05	1.05	6.53	5.76	2.97
10	0.74	0.43	7.52	6.20	5.49	0.49	4.42	3.73	2.30
20	0.93	0.48	6.37	5.18	5.15	0.15	3.09	2.47	1.88
100	1.20	0.55	5.29	4.25	4.84	-0.16	1.85	1.30	1.49
1000	1.28	0.56	5.03	4.02	4.76	-0.24	1.54	1.02	1.39

The initial conditions are: $\delta^{18}O = 5.0$ and $\delta^{17}O = 1.5$ ‰ for olivine and $\delta^{18}O = 21.0$ and $\delta^{17}O = 20.0$ ‰ for the gas. Other parameters and calculation method are same as in ref [19]. R: the dust/gas ratio, f_{SiO}: the fraction of O in the gas carried by SiO, $\delta^{18}O_{neb}$: $\delta^{18}O$ of the gas that was equilibrated with chondrule equilibrated, $\delta^{18}O_{SiO}$: calculated $\delta^{18}O$ value of the SiO gas, $\delta^{18}O_{pyroxene}$: calculated $\delta^{18}O$ of the pyroxene, and $\Delta^{18}O_{px\text{-}ol} = \delta^{18}O_{relict\ olivine} - \delta^{18}O_{pyroxene}$.

Supplementary Table 5 | Oxygen isotopic composition of reference San Carlos olivine.

reference number	weight (mg)	$\delta^{18}O$ (‰)	$\delta^{17}O$ (‰)	$\delta^{17}O^*$ (‰)	$\Delta^{17}O_{TSFL}$ (‰)
1	1.32	5.271 ±0.006	2.746 ±0.003	2.778	0.004 ±0.006
2	1.17	5.266 ±0.007	2.746 ±0.007	2.779	0.007 ±0.009
3	1.55	5.270 ±0.003	2.733 ±0.010	2.766	-0.008 ±0.009
4	1.64	5.243 ±0.005	2.727 ±0.004	2.760	0.000 ±0.002
5	1.28	5.364 ±0.007	2.782 ±0.007	2.815	-0.008 ±0.007
6	0.87	5.288 ±0.007	2.751 ±0.008	2.784	0.001 ±0.005
7	0.64	5.188 ±0.005	2.728 ±0.008	2.760	0.030 ±0.007
8	0.57	5.206 ±0.006	2.714 ±0.014	2.747	0.007 ±0.013
9	0.55	5.152 ±0.004	2.695 ±0.008	2.728	0.016 ±0.009
10	0.94	5.371 ±0.008	2.796 ±0.005	2.829	0.002 ±0.003
11	0.52	5.176 ±0.004	2.692 ±0.010	2.725	0.000 ±0.009
12	0.57	5.329 ±0.011	2.791 ±0.016	2.824	0.019 ±0.011
13	0.67	5.371 ±0.009	2.813 ±0.009	2.846	0.019 ±0.009
14	0.52	5.210 ±0.007	2.723 ±0.008	2.756	0.014 ±0.007
15	0.66	5.383 ±0.007	2.801 ±0.008	2.834	0.001 ±0.009
16	0.54	5.236 ±0.009	2.731 ±0.008	2.764	0.008 ±0.008
17	0.63	5.312 ±0.009	2.761 ±0.013	2.794	-0.002 ±0.012
18	0.71	5.233 ±0.002	2.720 ±0.009	2.753	-0.002 ±0.008
19	0.56	5.209 ±0.006	2.710 ±0.006	2.743	0.001 ±0.006
20	0.72	5.325 ±0.009	2.771 ±0.010	2.803	0.001 ±0.009
21	0.50	5.320 ±0.007	2.778 ±0.014	2.811	0.010 ±0.013
22	0.55	5.259 ±0.006	2.741 ±0.009	2.773	0.005 ±0.008
23	0.58	5.241 ±0.003	2.718 ±0.007	2.751	-0.007 ±0.008
24	0.56	5.318 ±0.005	2.774 ±0.007	2.807	0.008 ±0.006
25	0.54	5.260 ±0.005	2.742 ±0.007	2.775	0.007 ±0.006
26	0.66	5.299 ±0.009	2.745 ±0.007	2.778	-0.012 ±0.007
27	0.57	5.274 ±0.004	2.744 ±0.010	2.777	0.001 ±0.009
28	0.72	5.349 ±0.006	2.775 ±0.014	2.808	-0.007 ±0.011
29	0.65	5.406 ±0.006	2.799 ±0.013	2.832	-0.014 ±0.013
30	0.66	5.359 ±0.003	2.786 ±0.009	2.819	-0.001 ±0.009
31	0.83	5.357 ±0.010	2.794 ±0.010	2.827	0.007 ±0.010
32	0.53	5.295 ±0.003	2.750 ±0.009	2.782	-0.005 ±0.008
33	0.76	5.365 ±0.008	2.789 ±0.011	2.821	-0.002 ±0.009
34	0.51	5.371 ±0.006	2.795 ±0.005	2.828	0.001 ±0.006
35	0.52	5.375 ±0.010	2.793 ±0.010	2.826	-0.003 ±0.009
36	0.52	5.088 ±0.005	2.663 ±0.009	2.696	0.018 ±0.011
37	0.67	5.343 ±0.009	2.787 ±0.015	2.820	0.008 ±0.011
38	0.46	5.260 ±0.005	2.751 ±0.008	2.783	0.015 ±0.008
39	0.54	5.278 ±0.006	2.758 ±0.006	2.791	0.012 ±0.007
average ±1SD		**5.288 ±0.072**	**2.754 ±0.035**	**2.787**	**0.004 ±0.009**

Supplementary Table 6 | Isotopic composition of the San Carlos olivine-extracted oxygen in the presence of pyrrhotite during fluorination.

sample	weight (mg)		S/(S+O)	yield	$\delta^{18}O$	$\delta^{17}O$	$\Delta^{17}O_{TSFL}$
name	olivine	pyrrhotite	(in mol)	(%)	(‰)	(‰)	(‰)
$Ol_{96}Po_4$	1.60	0.06	0.032	98	5.276 ±0.003	2.745 ±0.010	-0.005 ±0.010
$Ol_{90}Po_{10}$	1.50	0.17	0.091	97	5.372 ±0.003	2.807 ±0.008	0.007 ±0.007
$Ol_{86}Po_{14}$	1.32	0.22	0.128	91	5.429 ±0.003	2.809 ±0.009	-0.021 ±0.008
$Ol_{83}Po_{17}$	1.56	0.31	0.149	90	5.489 ±0.004	2.832 ±0.012	-0.030 ±0.013
$Ol_{82}Po_{18}$	1.09	0.24	0.162	89	5.942 ±0.004	3.086 ±0.006	-0.015 ±0.007
$Ol_{80}Po_{20}$	1.36	0.34	0.180	88	5.434 ±0.005	2.820 ±0.004	-0.013 ±0.005
$Ol_{75}Po_{25}$	1.08	0.36	0.227	79	5.932 ±0.003	3.069 ±0.007	-0.026 ±0.006
$Ol_{70}Po_{30}$	1.45	0.62	0.273	74	5.952 ±0.003	3.074 ±0.008	-0.032 ±0.008
$Ol_{66}Po_{34}$	1.35	0.70	0.313	68	7.393 ±0.004	3.846 ±0.007	-0.019 ±0.007
$Ol_{50}Po_{50}$	1.51	1.51	0.468	54	8.140 ±0.004	4.214 ±0.006	-0.043 ±0.007